


Confronting theoretical results of localized and additional surface plasmon resonances in silver nanoparticles with electron energy-loss spectroscopy measurements

Guozhong Wang ^{*}*Department of Physics, College of Mathematics and Physics, Wenzhou University, Wenzhou 325035, China*

(Received 2 October 2020; revised 18 April 2021; accepted 21 April 2021; published 14 May 2021)

Raza *et al.* recently observed the extraordinarily large energy blueshifts of localized surface plasmon resonances and additional surface plasmon resonances in silver nanoparticles encapsulated in silicon nitride [S. Raza, S. Kadkhodazadeh, T. Christensen, M. D. Vece, M. Wubs, N. A. Mortensen, and N. Stenger, *Nat. Commun.* **6**, 8788 (2015)], which are not fully understood yet. By using the quantum model consisting of two subsystems, respectively, for describing the center of mass and intrinsic motions of conduction electrons of a metallic nanosphere and a coupling occurring between the center of mass and conduction electrons outside the metallic nanosphere, we first deduced the general energy and line broadening size dependence of localized surface plasmon resonances, which removes the divergent defect of usual $1/R$ size dependence. Second, we proposed that the additional surface plasmon resonance in a metallic nanosphere originates from the transition of the first excited state to the ground state of the center-of-mass subsystem with energy levels corrected by degenerate-state pairs of the system composed of the center of mass and intrinsic motions of conduction electrons. Then, we implemented this generation mechanism of additional surface plasmon resonances for silver nanoparticles encapsulated in silicon nitride, and the calculated results are consistent with experimental results. Furthermore, we obtained an energy expression of localized surface plasmon resonances, with which we successfully explained the extraordinarily large energy blueshifts of localized surface plasmon resonances in few-nanometer silver nanoparticles encapsulated in silicon nitride. Finally, we calculated the localized and additional surface plasmon resonance energies of silver nanoparticles resting on carbon films, and the calculated results perfectly explain the experimental measurements of Scholl *et al.* [J. A. Scholl, A. L. Koh, and J. A. Dionne, *Nature (London)* **483**, 421 (2012)]. Within this quantum model, the optical properties of metallic nanoparticles are completely determined by degenerate-state or nearly degenerate-state pairs of the system composed of the center-of-mass and intrinsic motions of conduction electrons. Our calculations also show that additional surface plasmon resonances play almost an equal role as localized surface plasmon resonances for metallic nanoparticles excited by fast-moving electrons.

DOI: [10.1103/PhysRevB.103.195417](https://doi.org/10.1103/PhysRevB.103.195417)

I. INTRODUCTION

Apart from the bulk plasmon resonance, the conduction electrons in a metallic nanoparticle (NP) support another, more important, self-sustaining collective oscillation, which is the well-known localized surface plasmon resonance (LSPR), and endow metallic NPs with particular abilities, such as local electromagnetic field rapid oscillation inside metallic NPs, colossal enhancement of local electric fields, extreme sensitivity to dielectric environment variations, and squeezing light beyond the diffraction limit [1,2]. These specialities of LSPRs render the manipulation of visible light waves at the nanoscales possible. Various applications continue to flourish in many areas, such as surface-enhanced Raman scattering [3], improvement of light confinement of photovoltaic devices [4], single-molecule detection [5], single-photon generation, and potential applications for quantum information transfer [6] and compact laser-driven accelerators [7]. It has also found applications in biochemistry and biomedical fields, such as

biosensing [8], drug delivery [9], and cancer phototherapy [10]. Recently, real-space and real-time observations of a plasmon-induced dissociated reaction of a single dimethyl disulfide molecule have been realized [11].

Paralleling with the explorations of deep physics of LSPRs, unique findings and ideas continue to emerge. Marinica *et al.* proposed a mechanism to actively control the optical response of metallic NPs by applying an external dc bias across a narrow gap [12]; Guzzinati *et al.* probed the symmetry of LSPRs with phase-shaped electron beams [13]; Roller *et al.* showed that coherent ultrafast nondissipative energy transfer could take place between two gold NPs with an interspaced silver island [14]. Such advances are boosted by the development of powerful nanoscale characterization techniques. Nowadays, electron energy-loss spectroscopy (EELS) combined with an electron monochromated and aberration-corrected scanning transmission electron microscopy is able to achieve energy resolution even down to 9 meV and ångström spatial resolution in the studies of individual plasmonic structures or dynamic imaging of clusters of a few atoms [15–19]. High energy and spatial resolutions of EELS in a scanning transmission electron

^{*}gzw@wzu.edu.cn

microscope also allow the studies of vibrational modes in nanostructures [20].

The LSPRs strongly depend on size, shape, temperature, material, and dielectric environment [21–25], which provides multiple variables tailorable for various applications. Silver nanostructures are ideal for plasmon studies owing to low intrinsic losses, narrow LSPR linewidths, and large optical field enhancements [15]. For metal silver, the fully occupied $4d$ bands described as a polarizable medium modify the frequency of the classical Mie plasmon resonance from $\omega_M = \omega_p / (1 + 2\epsilon_m)^{1/2}$ to $\omega_M = \omega_p / [\text{Re}(\epsilon_d) + 2\epsilon_m]^{1/2}$ [26,27], where $\omega_p = (4\pi\rho_e e^2/m)^{1/2}$ is the plasmon frequency of bulk metal, ϵ_m and ϵ_d , respectively, the dielectric constant of the environment and complex dielectric function of $4d$ bands; while e , m , and ρ_e are the electron charge, mass, and density, respectively. The localized $4d$ electrons fail to fully screen conduction electrons outside NPs, which prevails over the spill-out effect of conduction electrons and tends to blueshift the LSPR energies. Many different experiments have confirmed the LSPR energy blueshifts of silver NPs in various dielectric environments [28–31]. It is obvious that atomic configurations in the vicinity of the surface and spill-out effect of conduction electrons become more and more prominent with the particle size decreasing, which causes the optical properties of metallic NPs to be size dependent.

From the classical limited mean-free path effect or the calculation of dielectric constant of silver particles by using quantum methods, the LSPR linewidth is usually described by $\gamma(R) = \gamma_0 + g v_F / R$ [29,32–36], where R , v_F , and γ_0 are particle radius, Fermi velocity, and intrinsic linewidth. The dimensionless g is considered to be a constant, however, quite different values of g were obtained from experimental data and theoretical models [22,37]. The LSPR line broadening of metallic NPs is the result of exciting single particles into electron-hole states, which is the well-known Landau damping mechanism [36,38]. By using the generalized non-local optical response (GNOR) model, Mortensen *et al.* obtained a positive term $1/R^2$ for line broadenings and frequency shifts [39,40]. Based on experimental data [30], the self-energy approach for particle polarizability [41], and dispersion relation corrected by the spatial spreading of induced charge [42], the energy shifts of LSPRs were found to obey the same $1/R$ size dependence. However, this $1/R$ law suffers from the divergent defect for few-nanometer metallic NPs.

It has been well established that the LSPR is the dominant response mode for metallic NPs with radii less than 200 nm to external light excitation [22,43–45]. By using EELS, Raza *et al.* recently observed additional surface plasmon resonances (ASPRs) for silver NPs encapsulated in silicon nitride with radius range from 4 nm up to 20 nm [46], which were interpreted as the combined effect of many multipole surface plasmon resonances. While the ASPR disappearance of silver NPs with radii below 4 nm was ascribed to the decreasing of EELS signals from high-order modes. The measured ASPR energies of individual silver NPs do not have a constant value, and the multipole mode combination viewpoint of ASPRs fails to yield a feasible ASPR energy calculation method. Furthermore, except for the dipole surface plasmon resonance, there are no other individual multipole modes observed in their experiments.

Raza *et al.* also observed an extraordinarily large LSPR energy blueshift ~ 0.9 eV when the particle radius decreases from 4 nm to 1 nm [46]. Scholl *et al.* observed an energy blueshift ~ 0.5 eV for individual ligand-free silver NPs resting on carbon films [47], and a similar result was also observed for silver NPs dispersed on a silicon nitride substrate [48]. While the negligible energy blueshifts ~ 0.25 eV appeared for silver NPs embedded in solid Xe, Ar, and C_2H_4 [29,30]. These experimental results show that the LSPR energy blueshifts of silver NPs strongly depend on their surroundings. Besides the screening effect of $4d$ electrons and the spill-out effect of conduction electrons, it is believed that the stronger quantum confinement, single-particle excitations, nonlocal response, and numerous structural surface defects are the possible factors jointly determining the energy blueshifts of silver NPs [21,43]. To understand the extraordinarily large LSPR energy blueshifts of silver NPs is an arena to test various models or theories. To the best of our knowledge, all theoretically predicted energy blueshifts of silver NPs are systematically less than experimental results [31,48].

Nowadays, the understanding of LSPR energy shifts of metallic NPs is still poor. Quantitative predictions require the full consideration of quantum effects, which become more and more important with the particle size decreasing. The time-dependent density functional theory (TD-DFT) offers the possibility to address the optical response of plasmonic systems at the quantum *ab initio* level [49,50]. However, the TD-DFT becomes computationally prohibitive because their computational cost grows as fast as $O(N^3)$, such that their reach is limited to systems with a few thousands of electrons, where N is the total number of conduction electrons contained in nanostructures. The semiclassical hydrodynamic Drude models (HDMs) deal with differential equations of macroscopic particle density and current density rather than single electron orbitals gaining the advantage of numerical efficiency compared with TD-DFT, which manifests the HDMs as a promising tool suitable to study the optical properties of large plasmonic structures. By adding the second-order conduction electron density gradient correction, the von Weizsäcker functional, to the Thomas-Fermi kinetic functional, such HDMs are called quantum hydrodynamic theories (QHTs) in the literature, and the hard-wall boundary condition of HDMs can be removed and the spill-out effect can be considered. For example, the self-consistent QHT is able to give accurate ground-state and excited-state properties of an inhomogeneous electron gas [51]. By assuming electrons in different states mutually collide, a viscous stress tensor yielding a dynamical correction to the kinetic energy functional is expected to play the role of the Landau damping mechanism [52]. It is believed that QHTs combined with suitable electron ground-state density are able to compete with the TD-DFT [53]. However, it is still challenging to build a QHT compatible with all experimental findings [54].

If the optical properties of metallic nanostructures with simple configurations were known, it would be helpful to understand the optical properties of multiscale plasmonic systems composed of these simple blocks, such as the dimmers made from two closely coupled metallic nanowires and the honeycomb lattices of metallic NPs [55,56]. Therefore, a thorough understanding of basic systems can facilitate the design

of highly sophisticated plasmonic nanostructures with desired optical properties.

In this paper, we will use a quantum model specially constructed for metallic nanospheres to solve some unfathomed problems associated with silver NPs.

II. THE QUANTUM MODEL

For metallic NPs, the ionic cores can be treated as a uniform positively charged background according to the jellium model [57], which is extensively adopted in numerous theoretical models, such as TD-DFT [58], the matrix random-phase approximation method [59], and field theory of quantum plasmonics [60]. Due to strong quantum confinement, conduction electron states are quantized into discrete levels. For a metallic nanosphere containing N atoms with radius R encapsulated in the medium with dielectric constant ϵ_m , based on the jellium model one can construct a quantum model by separating the conduction electron coordinates into the coordinate of center of mass and the relative coordinates (SCRM). The total Hamiltonian \mathcal{H}_T of the SCRM can be expressed as the sum of two sub-Hamiltonians \mathcal{H}_C and \mathcal{H}_r , respectively, for describing the collective and intrinsic motions of conduction electrons, and the coupling \mathcal{H}_c between the center of mass and conduction electrons outside the nanosphere, they, respectively, are [61,62]

$$\begin{aligned}\mathcal{H}_C &= \sum_{(n)} (n + 1/2) \hbar \Omega_p \hat{b}^\dagger \hat{b}, & \mathcal{H}_r &= \sum_{|\alpha\rangle} \epsilon_\alpha \hat{c}_\alpha^\dagger \hat{c}_\alpha, \\ \mathcal{H}_c &= \mathcal{A} (\hat{b}^\dagger + \hat{b}) \sum_{|\alpha, \beta\rangle} d_{\alpha\beta} \hat{c}_\alpha^\dagger \hat{c}_\beta,\end{aligned}\quad (1)$$

where \hat{b}^\dagger and \hat{b} are the creation and annihilation operators of harmonic oscillator and their definitions can be found in Ref. [63]; the ϵ_α and \hat{c}_α^\dagger (\hat{c}_α) are the eigenenergies and creation (annihilation) operators associated with one-body eigenstates $|\alpha\rangle$ determined by the effective potential V_{eff} confining conduction electrons. The sub-Hamiltonian \mathcal{H}_C has the standard harmonic oscillator structure with the frequency $\Omega_p = \omega_s \sqrt{1 - N_{\text{out}}/N}$, where ω_s is the unique input parameter of the SCRM and slightly varies around the classical Mie resonance frequency ω_m due to numerous surface structural defects, N_{out} the number of conduction electrons outside the nanosphere, and the coefficient $\mathcal{A} = \frac{e^2}{4\pi\epsilon_0 R^3} \sqrt{\frac{\hbar N}{2m\Omega_p}}$. The matrix element $d_{\alpha\beta}$ calculated between two states $|\alpha\rangle$ and $|\beta\rangle$ of \mathcal{H}_r is [63]

$$d_{\alpha\beta} = \langle \alpha | \xi_z (R^3 / |\vec{\xi}|^3 - 1) \Theta(|\vec{\xi}| - R) | \beta \rangle,$$

where $\Theta(x)$ is the Heavyside step function, $\vec{\xi}$ the relative coordinates of conduction electrons. To construct the SCRM, the electrostatic potential between a single electron and the ionic background is expanded to the second order of the coordinate of the center of mass, which is the only approximation in the SCRM. Because the magnitude of the displacement of the center of mass of conduction electrons is much less than the particle size, the SCRM is in essence quite precise to study the optical properties of metallic NPs.

Within the mean-field approximation, the energy levels and corresponding wave functions of conduction electrons can be

obtained by solving the Kohn-Sham equation,

$$\left[-\frac{\hbar^2}{2m} \nabla^2 + V_{\text{eff}}(|\vec{\xi}|) \right] \psi_\alpha(\vec{\xi}) = \epsilon_\alpha \psi(\vec{\xi}), \quad (2)$$

where the effective potential V_{eff} , usually including ionic background potential, Hartree potential, and exchange and correlation potentials, can be obtained by local density approximation calculation [57,63]. The quantum states of the total Hamiltonian \mathcal{H}_T can be expressed as $|I, \alpha\rangle$, where I and α are the quantum numbers, respectively, characterizing the states of the center of mass and intrinsic motions of conduction electrons. Within the SCRM, the expression of the LSPR frequency is easily derived from perturbation theory and the result is [63]

$$\Omega_q(R) = \Omega_p(R) + \frac{2\mathcal{A}^2}{\hbar} \sum_{|\alpha, \beta\rangle} \mathcal{F}_\alpha f_\beta \frac{|d_{\alpha\beta}|^2 \epsilon_{\beta\alpha}}{\epsilon_{\alpha\beta}^2 - (\hbar\Omega_p)^2}, \quad (3)$$

where the sum is over all the nondegenerate state pairs $\{|0, \alpha\rangle, |1, \beta\rangle\}$ of the total Hamiltonian \mathcal{H}_T with $0 < \epsilon_\alpha - \epsilon_\beta = \epsilon_{\alpha\beta} \neq \hbar\Omega_p$ and the corresponding $|d_{\alpha\beta}| \neq 0$; $f_\beta = 1/(1 + e^{(\epsilon_\beta - \mu)/k_B T})$ the Fermi-Dirac distribution; T , k_B , and μ the electronic temperature, the Boltzmann constant, and the chemical potential, respectively. We define $\mathcal{F}_\alpha = 1 - f_\alpha$. The conduction electron energy levels explicitly appear, especially in the denominator of Eq. (3), and negligible changes of energy levels would yield non-negligible deviation. Therefore, Eq. (3) is too sensitive to the energy levels of conduction electrons to be virtually useful unless precise enough energy levels of conduction electrons are obtained by strictly solving Eq. (2).

The line broadening of LSPRs caused by the Landau damping mechanism is [63]

$$\hbar\gamma(R) = 2\pi \mathcal{A}^2 \sum_{|\alpha, \beta\rangle} \mathcal{F}_\alpha f_\beta |d_{\alpha\beta}|^2 \delta(\epsilon_{\alpha\beta} - \hbar\Omega_p), \quad (4)$$

where $\delta(\epsilon_{\alpha\beta} - \hbar\Omega_p)$ is Dirac's δ function representing the condition of energy conservation.

For a sodium nanosphere containing 1760 atoms, the LSPR frequency and line broadening calculated by using the SCRM are perfectly consistent with the results of TD-DFT calculations [61], which indicates that the SCRM is really reliable to study the optical properties of metallic NPs.

III. THE LSPR ENERGY SIZE DEPENDENCE

The LSPR energy and linewidth are of crucial significance in many applications and intrinsically limit the optimization of nanosized optical devices involving metallic NPs. Within the SCRM, the LSPR energy shift and line broadening are determined by the energy states of conduction electrons and the input parameter ω_s , which include all effects of material, shape, size, dielectric environment, and surface details, such as facets and vertices [64]. The energy levels and wave functions of conduction electrons can be obtained, in principle, by solving Eq. (2). Thus, the effective potential of conduction electrons plays a central role in the optical properties of metallic NPs. However, the real effective potential confining conduction electrons is so complex that to obtain precise enough energy levels and numerical wave functions from Eq. (2) is extremely

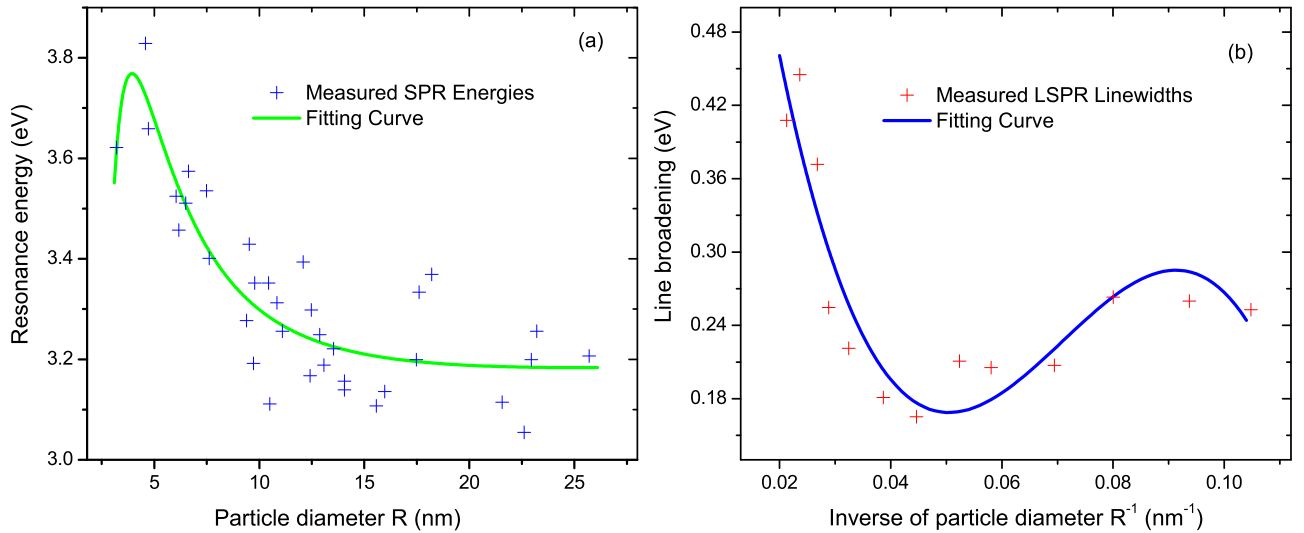


FIG. 1. (a) Surface plasmon resonance energies (blue crosses) measured in the EELS experiment for silver NPs dispersed on a silicon nitride substrate [48]. The fitting function is $\hbar\Omega_q(R) = 3.25 - 3.46/R + 51.56/R^2 - 117.51/R^3$, which is indicated by the green line. (b) Measured linewidths of localized surface plasmon resonances (red crosses) of individual silver NPs coated with a silica shell [22]. The fitting function is $\hbar\gamma(R) = 1.14 - 47.39/R + 729.06/R^2 - 3428.79/R^3$, which is indicated by the blue curve.

time-consuming and quickly becomes prohibitive with the particle size increasing, which is the very reason for the exploration of other calculation schemes without resorting to single energy levels and wave functions.

Equations (3) and (4) show that the size dependences of the LSPR energy shift and line broadening are determined by the product of matrix elements $|d_{\alpha\beta}|^2$ and the coefficient \mathcal{A}^2 and have the same form. Within the SCRM, the general size dependence of LSPR energies and linewidths can be derived and the expression is [65]

$$f(R) = f_0 + \frac{E}{R} + \frac{K}{R^2} + \frac{S}{R^3}. \quad (5)$$

Besides the first two terms, two high order terms of $1/R$ arise, which completely originate from quantum effects and are able to eliminate the divergent defect of the usual size dependence $1/R$ for tiny metallic NPs. The constant f_0 is the intrinsic linewidth γ_0 or the classical Mie plasmon resonance frequency ω_M . Following the usual expression of the coefficient $E = g_1 v_F$, the coefficients K and S can be, respectively, expressed as $g_2 v_F^2 / \omega_M$ and $g_3 v_F^3 / \omega_M^2$. Because the classical Mie frequency ω_M includes the main influence of dielectric environments, we can expect that g_1 , g_2 , and g_3 are approximate constants without dimensions.

Figure 1 shows the fits of Eq. (5) to measured plasmon energies of silver NPs dispersed on a silicon nitride substrate [48] and linewidths of individual silver NPs coated with a silica shell [22]. The fitting curves are able to globally describe the experimental data, especially for the linewidths in Fig. 1(b). The large energy spread of plasmon resonances shown in Fig. 1(a) is related to the fact that part of the experimental data are ASPR energies and the ASPR and LSPR energies do not obey the same size dependence.

The optical properties of metallic NPs are extremely sensitive to the surface atomic configurations. The chemical control of surface layers via ligand exchange could yield abnormal

optical response behaviors [66], which shows that the electron density tail plays a crucial role in the optical response of metallic NPs. In deducing Eq. (5), the possible chemical bonding processes occurring between the surface atoms of metallic NPs and external molecules, which is able to dramatically alter the spatial distribution of conduction electron density tail, interfacial dielectric constant, and the effective potential, were not considered. Therefore, Eq. (5) cannot describe the LSPR size evolution behavior of metallic NPs in complex chemical environments.

IV. THE ASPRS OF METALLIC NPS

The ASPR was first identified as a surface mode for a semi-infinite metal by Bennett with hydrodynamic equations [67], and appeared in microscopic calculations for sodium particles [41,58]. However, the generation mechanism of ASPRs is still unclear so far, and many quite different viewpoints of ASPRs exist. For examples, Raza *et al.* regard the ASPR in silver NPs as the merger of many multipole modes [46]; Liebsch believed that the ASPR is the excitation that has dipolar angular character but with an additional node in the radial distribution of the dynamical surface screening charge compared to that of the principal Mie plasmon oscillation [41]; while Tsuei *et al.* deemed the ASPR the resonance in the electron-hole pair spectrum and no longer bearing purely dipolar character [68]. Unlike the LSPRs, the ASPRs have neither been extensively investigated nor attracted much attention until recently.

It is surprising that there exists a simple generation mechanism of ASPRs within the SCRM. For a degenerate-state pair $\{|0, \alpha\rangle, |1, \beta\rangle\}$ with $\epsilon_\alpha \sim \hbar\Omega_p + \epsilon_\beta$, the perturbation energy correction to states $|0, \alpha\rangle$ and $|1, \beta\rangle$ is easy to calculate and the result is $\pm\mathcal{A}|d_{\alpha\beta}|$ for $|0, \alpha\rangle$ and $\mp\mathcal{A}|d_{\alpha\beta}|$ for $|1, \beta\rangle$. Because the sub-Hamiltonian \mathcal{H}_C describes the collective motions of all conduction electrons, the perturbation energy correction to each state of a degenerate-state pair is virtually the correction

to states of \mathcal{H}_C . It seems that these two sets of energy corrections to the ground state $|0\rangle$ and the first excited state $|1\rangle$ of \mathcal{H}_C with opposite signs would offset each other and produce zero results. However, the positive energy correction $\mathcal{A}|d_{\alpha\beta}|$ to the ground state $|0\rangle$ would increase the collective oscillation energy of conduction electrons, which violates the principle that the ground state of a system would have the energy as low as possible. Therefore, the ultimate result of perturbation energy correction of the degenerate state pair $\{|0, \alpha\rangle, |1, \beta\rangle\}$ is $-\mathcal{A}|d_{\alpha\beta}|$ for the ground state $|0\rangle$ and $\mathcal{A}|d_{\alpha\beta}|$ for the first excited state $|1\rangle$. Thus, all degenerate-state pairs would yield a new surface plasmon resonance with the energy given by the expression

$$\hbar\Omega_\alpha(R) = \hbar\Omega_p(R) + 2\mathcal{A} \sum_{\{\alpha\beta\}} \mathcal{F}_\alpha \mathcal{F}_\beta |d_{\alpha\beta}|, \quad (6)$$

where the sum is over degenerate-state pair set $\{|0, \alpha\rangle, |1, \beta\rangle\}$. It is natural to think of this new surface plasmon resonance as the ASPR because in metallic NPs there only exist three kinds of plasmon resonances, namely, the LSPR, ASPR, and bulk plasmon resonance.

For a metallic NP with radius R less than 20 nm encapsulated in homogeneous dielectric medium, the single-particle effective potential V_{eff} determining quantum states of conduction electrons is not only complex but hard to obtain. Compared with Eq. (3), the energy levels and wave functions of conduction electrons only indirectly appear in Eq. (6) through distribution functions and matrix elements, which indicates that Eq. (6) is much less sensitive to energy levels of conduction electrons.

It has been shown that most of the energy levels and wave functions of the Schrödinger equation with a Woods-Saxon-like potential are almost the same as those of the spherical potential well of finite depth [69], and the observable difference between corresponding energy levels of two potentials focuses on the energy levels well above the Fermi energy. However, the contribution of states with high energy levels to Eq. (6) is suppressed by the Fermi-Dirac distribution factor. On the other hand, the wave functions of spherical potential well of finite depth decay slightly faster well outside the metallic nanosphere than those of Woods-Saxon-like potential well. However, the deviations of matrix elements calculated by using wave functions of the spherical potential well of finite depth from precise results are negligible for not-very-small nanospheres. Therefore, the spherical potential well of finite depth equal to the sum of Fermi energy and work function is able to substitute for the complex single-particle effective potential to calculate the ASPR energy of a metallic nanosphere.

There are no quantum states strictly satisfying the condition $\epsilon_\alpha = \epsilon_\beta + \hbar\Omega_p$, thus the main obstacle to calculate the ASPR energies by using Eq. (6) is how to single out all degenerate-state pairs from possible quantum states $|0, \alpha\rangle$ and $|1, \beta\rangle$. The energy levels of conduction electrons can be broadened out according to the formula [70]

$$\mathcal{E}(\epsilon, \epsilon_\alpha) = \frac{2}{\pi} \frac{\sqrt{\epsilon_r \epsilon_\alpha}}{(\epsilon - \epsilon_\alpha)^2 + 4\epsilon_r \epsilon_\alpha}, \quad (7)$$

where $\epsilon_r = (\hbar k_0)^2 / 2m$, and $k_0 = 0.13N^{-1/3} \text{Å}^{-1}$. Thus, the width of an energy level changes from zero to $2\sqrt{4\epsilon_r \epsilon_\alpha}$.

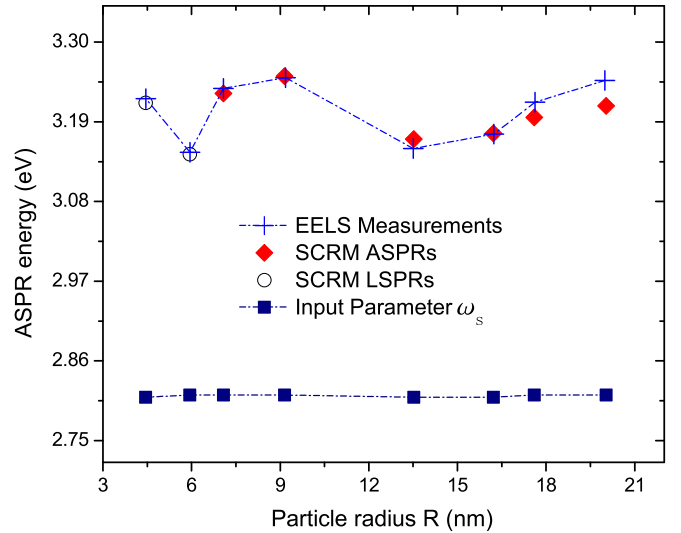


FIG. 2. The ASPR energy of silver NPs encapsulated in homogeneous silicon nitride versus the particle radius. Blue crosses and red squares, respectively, denote measured ASPR energies displayed in Fig. 5 of Ref. [46] and calculated ASPR energies. The first two measured ASPR energies perfectly correspond to the calculated LSPR energies indicated by black empty circles. The blue squares of the lower panel denote the values of the input parameter $\hbar\omega_s$ for corresponding silver NPs.

We define truly degenerate-state pairs (TDSPs) and nearly degenerate-state pairs (NDSPs) responsible for ASPR energies and LSPR energy shifts as state pairs with energies, respectively, satisfying

$$|\hbar\Omega_p - |\epsilon_{\alpha\beta}|| \leq \mathcal{A}|d_{\alpha\beta}| \quad (8)$$

and

$$|\hbar\Omega_p - |\epsilon_{\alpha\beta}|| \leq (\sqrt{4\epsilon_r \epsilon_\alpha} + \sqrt{4\epsilon_r \epsilon_\beta}). \quad (9)$$

According to the SCRM, the ASPRs originate from the degenerate-state pairs of the system. To test this viewpoint, we calculated the ASPR energies of silver NPs encapsulated in silicon nitride under the same settings of experiments done by Raza *et al.* [46]. The conduction electron temperature is fixed at the room temperature $T = 300$ K in all our calculations, and the Mie plasmon resonance frequency is calculated by using the measured frequency-dependent complex dielectric function of $4d$ band for bulk silver $\epsilon_d(\omega) = (59.8 + 55.1i)(\omega/\omega_p)^2 - (40.3 + 42.4i)(\omega/\omega_p) + (10.05 + 8.06i)$ [48]. By taking the experimental value 3.3 of environment dielectric constant ϵ_m [46], we obtained the Mie plasmon resonance energy $\hbar\omega_m = 2.8076$ eV. The calculated and measured ASPR energies are exhibited in Fig. 2, which shows a good agreement between calculated and experimental results. Thus, we can preliminarily conclude that both the generation mechanism and calculation scheme of ASPRs based on the SCRM are reasonable. For large silver NPs, Fig. 2 shows explicit discrepancies between calculated and measured ASPR energies, which contradicts with the predictive capability of the SCRM that, the larger the metallic NPs, the better the calculated results. These discrepancies occurring for large silver NPs, in turn,

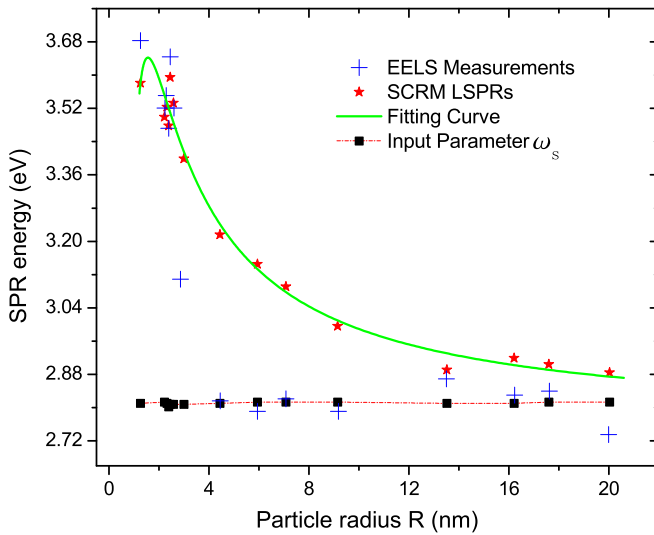


FIG. 3. The LSPR energy of silver NPs encapsulated in silicon nitride versus the particle radius. The blue crosses and red pentagrams, respectively, denote measured LSPR energies by Raza *et al.* [46] and calculated LSPR energies. The green curve indicates the fitting function $\hbar\Omega_q(R) = 2.7534 + 2.4960/R - 1.3177/R^2 - 0.6452/R^3$ of Eq. (5) to calculated LSPR energies. The blue squares of the lower panel denote the values of the input parameter $\hbar\omega_s$ for corresponding silver NPs. In this experimental settings, the input parameter $\hbar\omega_s$ remains almost invariable for different silver NPs.

show that the perfect agreement between four calculated and four experimental ASPR energies in the middle of Fig. 2 is somewhat coincidental. The first two measured ASPR energies of silver NPs with radii 4.44 nm and 5.94 nm on the left side of Fig. 2 are not consistent with calculated ASPR energies. However, these two measured surface plasmon resonances can be explained as the LSPRs.

In principle, the SCRM generation mechanism of ASPRs predicts the existence of ASPRs for almost all the metallic NPs. Because there are no or few TDSPs for few-nanometer metallic NPs, the ASPR energies normally shift from high ASPR energies of large metallic NPs to low energies [$\sim\hbar\Omega_p(R)$], according to Eq. (6). This behavior of ASPRs naturally explains the experimental observation that the ASPRs in few-nanometer silver NPs encapsulated in silicon nitride fail to be observed at the high-energy region containing the ASPRs of large silver NPs [46]. Whether or not the ASPRs in few-nanometer metallic NPs are experimentally observable strongly depends on the intensity ratio of ASPRs to background signals. The ASPR energies ~ 2.80 eV in silver NPs with radii 4.44 nm and 5.94 nm, and ~ 3.11 eV for silver NPs with radius 3.0 nm were observed, which are shown in Fig. 3 and are mistaken for the LSPR energies by Raza *et al.* [46]. These experimental results are consistent with the SCRM predictions.

However, the SCRM generation mechanism of ASPRs does not exclude the occasional appearance of ASPRs with large resonance energies for few-nanometer metallic NPs with special sizes. Actually, for the silver NPs encapsulated in silicon nitride with radius $R \sim 2.62$ nm and the input parameter $\hbar\omega_s$ ranging from 2.795 eV to 2.822 eV, the ASPR energies vary from 3.23 eV to 3.29 eV even larger than those of large

silver NPs. Small sodium clusters with special sizes are also able to support the ASPRs shown by the surface loss function and dynamical polarizability calculated, respectively, by using time-dependent density-functional approach and local-density approximation method [41,58], which indirectly shows that the SCRM generation mechanism of ASPRs in metallic NPs is reasonable.

When the radius of metallic NPs increases from a few nanometers to tens of nanometers, the ASPR energy generally increases from $\sim\hbar\Omega_p(R)$ to high ASPR energies of large metallic NPs. When the particle radius further increases to macroscopic sizes, how does the ASPR in metallic particles evolve? Figure 2 shows that the ASPRs in silver NPs with macroscopic sizes seem to remain the ASPR energies of large silver NPs. However, according to the SCRM generation mechanism, the size dependence of ASPR energies determined by the coefficient \mathcal{A} and matrix elements $|d_{\alpha\beta}|$ calculated between degenerate-state pairs varies with the particle radius as $\sim 1/\sqrt{R}$ [65]. Therefore, the ASPR together with the LSPR in metallic NPs would evolve into the classical Mie surface plasmon resonance with the particle size increasing to macroscopic sizes. This evolving mode of surface plasmon resonances is also given by the classical electrodynamics combined with the measured dielectric function for metallic particles excited by fast-moving electrons [71,72].

The large energy spread of surface plasmon resonances for silver NPs resting on different substrates was observed in EELS experiments [47,48]. Besides shape variations, facets, and the interaction between particles and the substrates, it is undoubted that the ASPRs play a significant role in measured large energy spreads of surface plasmon resonances.

V. THE LSPR ENERGY SHIFTS

Precise EELS experiments explicitly show that the LSPR energies of few-nanometer silver NPs shift to higher energies by remarkable deviations from the classical Mie surface plasmon resonance energy [46–48]. The EELS measurements also indicate that the blueshifts of LSPR energies toward higher energies are not purely monotonic but with a greater variety in peak locations when the particle size decreases to few nanometers. Both relatively small amplitude and monotonic behavior of LSPR energies predicted by known theories and models show that the LSPR energy shift of metallic NPs is poorly understood, and the extraordinarily large energy blueshifts for small silver NPs have not been satisfactorily interpreted so far [31,47,48]. If extremely powerful computation ability were possessed in the future, the TD-DFT would yield the LSPR energies of metallic NPs perfectly consistent with experimental measurements. Likewise, once the sufficiently precise energy levels and wave functions were available, we also believe that the frequency expression Eq. (3) would produce correct results of metallic NPs. However, Eq. (3) is too sensitive to conduction electron energy levels to produce the correct results by using the energy levels of the spherical potential well of finite depth. Fortunately, Eq. (3) can be transformed into an alternative form by some mathematical manipulations, which greatly lowers its sensitivity to conduction electron energy levels. The new expression of LSPR

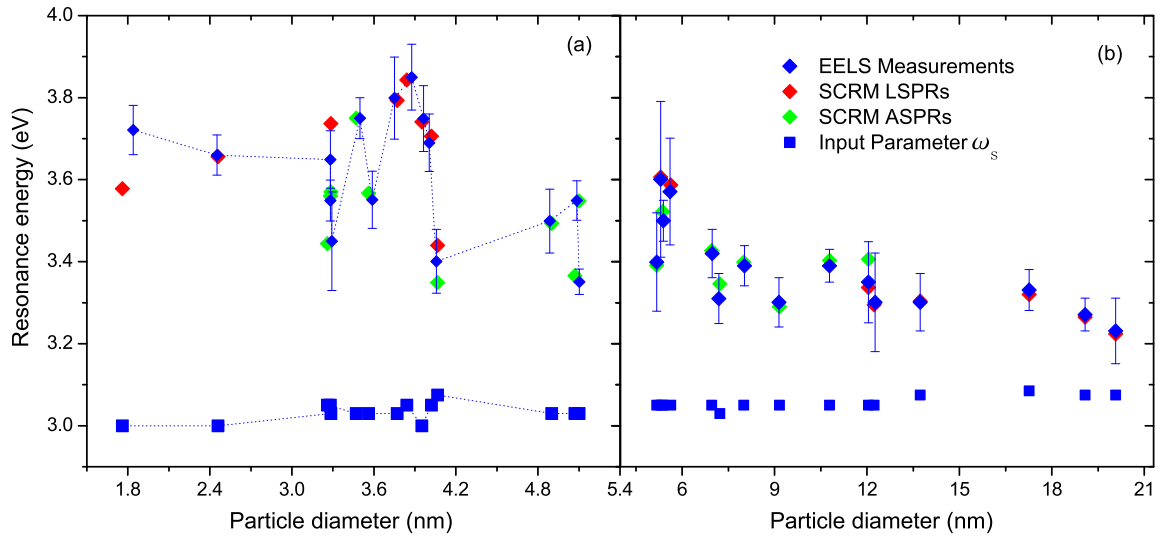


FIG. 4. The surface plasmon resonance energy versus the particle diameter. The blue, red, and green squares, respectively, denote measured plasmon energies by Scholl *et al.* [47], calculated energies of LSPRs and ASPRs. The black squares denote the values of the input parameter $\hbar\omega_s$ for corresponding silver NPs. For clarity, all data are depicted in two plots, (a) and (b).

energies is (detailed derivation see Appendix)

$$\hbar\Omega_q(R) = \hbar\Omega_p(R) \pm \frac{\pi\mathcal{A}^2}{\tau} \sum_{\{\alpha\beta\}} (f_\beta - f_\alpha) |d_{\alpha\beta}|^2, \quad (10)$$

where the signs $+$ and $-$, respectively, for the LSPR energy blueshifts and redshifts; the sum is over NDSPs with $\epsilon_\alpha > \epsilon_\beta$ and $d_{\alpha\beta} \neq 0$. However, there are a small number of NDSPs not contributing to the LSPR energies expressed in Eq. (10), and such NDSPs should be excluded [73]. For silver NPs encapsulated in silicon nitride, we calculated the LSPR energies of silver NPs, which are measured by Raza *et al.* in the EELS experiments [46]. All the calculated LSPR energies and experimental counterparts are exhibited in Fig. 3. Nevertheless, for silver NPs with radii larger than 2.58 nm, our calculated results are not consistent with measured ones. We think that this inconsistency is induced by the improper identification of the LSPRs and ASPRs and their energies from EELS spectra [46]. For silver NPs with radii smaller than 2.58 nm, only LSPRs were observed in the EELS spectra, and our calculated results are perfectly consistent with experimental measurements naturally explaining the extraordinarily large LSPR energy blueshifts measured by Raza *et al.* for few-nanometer silver NPs [46]. Furthermore, we found that our calculated LSPR energies are well described by the general LSPR energy size dependence Eq. (5), which is also shown in Fig. 3. It is obvious that the measured LSPR energies by Raza *et al.* for silver NPs encapsulated in silicon nitride shown in Fig. 5 of Ref. [46] failed to obey this rule, which should perfectly follow the size dependence of LSPR energies.

To further test the SCRM generation mechanism of ASPRs and the LSPR calculation formula Eq. (10), we calculated the LSPR and ASPR energies of individual silver NPs resting on carbon films, which were first studied in the EELS experiments by Scholl *et al.* [47]. Although metallic NPs encapsulated in a homogeneous dielectric medium and resting on substrates are quite different experimental settings,

the theoretical treatments are the same. The background of metallic NPs of the former situation is described by a constant permittivity, while the latter situation being inhomogeneous could be described by an effectively constant permittivity. The constant or effective constant permittivity determines the classical Mie resonance energy of metallic NPs. We noticed that the larger the particle size, the smaller the influence of carbon films on the effective dielectric constant ϵ_m . Therefore, we can expect that the input parameter $\hbar\omega_s$ for silver NPs resting on carbon films would exhibit a larger variation amplitude than that of silver NPs encapsulated in homogeneous silicon nitride. According to the proposed effective dielectric constant $\epsilon_m = 1.69$ [47], the corresponding Mie plasmon resonance energy $\hbar\omega_m = 3.373$ eV is even larger than the measured LSPR energies of silver NPs with diameters ~ 20 nm. Because the LSPR energy of silver NPs blueshifts with the particle size decreasing, this proposed effective dielectric constant is obviously unreasonable. In our calculations, the input parameter $\hbar\omega_s$ varies in the range $3.0 \text{ eV} < \hbar\omega_s < 3.085 \text{ eV}$. The calculated energies of LSPRs and ASPRs are shown together with measured results in Fig. 4. Most of the measured plasmon resonances (blue squares) perfectly correspond to either calculated LSPRs (red squares) or ASPRs (green squares). There also exists another situation. For a silver NP with special sizes, the calculated peak locations of the LSPR and ASPR happen to be so close to each other that they virtually merge into one peak and are indistinguishable in EELS experiments. We found that three measured plasmon resonances could be perfectly explained as such merged peaks, which are indicated by arrows in Fig. 4. We found that in this EELS experiment by Scholl *et al.*, more than half the measured surface plasmon resonances are ASPRs for silver NPs with the particle diameter ranging from 3.2 nm to 12 nm. Beyond this range, all measured plasmon resonances can be explained as LSPRs.

When a silver NP has a diameter less than 2.0 nm, conduction electrons have considerable possibility to stay outside the silver NP. To substitute the spherical potential well of

finite depth for the effective potential confining conduction electrons begins to deteriorate, which is the reason why the first calculated LSPR energies of Figs. 3 and 4 are explicitly smaller than experimental results. Therefore, within the SCRM, one has to use more precise energy levels and wave functions of conduction electrons to calculate LSPR energies of metallic NPs with radii below 1.5 nm.

Much larger LSPR energy blueshifts from 0.8 eV to 1.2 eV appeared in our calculations for silver NPs resting on carbon films with diameters in the ranges $3.26 \text{ nm} < D < 3.32 \text{ nm}$ and $3.44 \text{ nm} < D < 3.50 \text{ nm}$.

VI. DISCUSSION

By using the SCRM, we obtained the general size dependence of LSPR energies and linewidths for metallic NPs encapsulated in homogeneous medium. Besides the LSPR and volume plasmon resonance, the ASPR is another significant surface plasmon resonance of metallic NPs. Based on the SCRM, we proposed that the ASPR of a metallic nanosphere originates from all the TDSPs of the system composed of the center-of-mass and intrinsic motions of conduction electrons. Then, we implemented this SCRM generation mechanism of ASPRs in silver NPs encapsulated in silicon nitride and explained the ASPRs measured by Raza *et al.*, which shows that the SCRM generation mechanism of ASPRs is reasonable. The ASPRs in metallic NPs are completely induced by quantum effects and would evolve into the classical Mie plasmon resonance when the particle size increases to macroscopic sizes. The SCRM generation mechanism shows that the ASPRs in metallic NPs almost always exist. For few-nanometer metallic NPs, the ASPRs generally do not disappear but shift their peak locations to low energy region $\sim \hbar\Omega_p$, which is supported by measured ASPR energies ($\sim 2.8 \text{ eV}$) of silver NPs encapsulated in silicon nitride with radii 4.44 nm and 5.94 nm.

Within the SCRM, the LSPR of a metallic NP is determined by the transition from the first excited state $|1\rangle$ to the ground state $|0\rangle$ of the center of mass of conduction electrons with these two energy levels corrected by all nondegenerate states of the system. There are no essential differences between the origins of the LSPR and ASPR in metallic NPs. Therefore, it is somewhat strange that LSPRs can be excited by both lights and fast-moving electrons, while the ASPRs can only be excited by fast-moving electrons. To the best of our knowledge, there are indeed no reports of ASPRs observed in experiments by using lights to excite plasmon resonances. There are several possible reasons for the ASPRs unobserved in the light excitation experiments, such as relatively low experimental precision, the light energy range being too narrow to cover LSPR and ASPR peaks, or the peak locations of the ASPR and LSPR being too close to be distinguished. It is well known that the LSPR energies of sodium NPs redshift, while the ASPR energies generally blueshift. Therefore, it seems most likely to observe the ASPRs in light excitation experiments of sodium NPs encapsulated in transparent medium.

It is usually considered that the optical properties of metallic NPs are functions of the particle size. For silver NPs resting on a silicon nitride substrate with the same size, the EELS measurements show that the amplitude and linewidth

of the surface plasmon resonances can vary from particle to particle [48]. Within the SCRM, it is natural to regard the LSPR and ASPR energies and line broadenings as the functions of the particle radius R and input parameter $\hbar\omega_s$. In a general way, the input parameter $\hbar\omega_s$ can be expressed as $\hbar\omega_s = \hbar\omega_M [1 - \delta\epsilon_m / (\text{Re}(\epsilon_d) + 2\epsilon_m)]$, where the quantity $\delta\epsilon_m$, the deviation from the dielectric constant ϵ_m of the dielectric medium encapsulating metallic NPs, can be further expressed as $\delta\epsilon_m = \delta\epsilon_c + \delta\epsilon_d + \delta\epsilon_s$, and these three terms are, respectively, induced by atomic configurations in the vicinity of surfaces, shape deviation from perfect spheres, and effects related to the size of individual metallic NPs. The first two terms in the expression of $\delta\epsilon_m$ generally exist, but the third term $\delta\epsilon_s$ depends on experimental settings. For metallic NPs encapsulated in a homogeneous medium, the first two terms $\delta\epsilon_c$ and $\delta\epsilon_d$ are the main effects causing the input parameter $\hbar\omega_s$ to be different from the Mie surface plasmon resonance energy $\hbar\omega_M$, while for metallic NPs resting on a substrate, the inhomogeneous dielectric environments and the interactions between metallic NPs and the substrate render the term $\delta\epsilon_s$ significant, which is the reason why the variation amplitude of the input parameter for silver NPs resting on carbon films is evidently larger than that of silver NPs encapsulated in silicon nitride. It is obvious that the input parameter $\hbar\omega_s$ has different values for different metallic NPs even with the same size leading to different TDSP and NDSP sets through $\hbar\Omega_p$ according to Eqs. (8) and (9), which would yield different energies and line broadenings of LSPRs and ASPRs. The larger the variation of the input parameter, the larger the variation of LSPR and ASPR energies and line broadenings, which naturally explains the experimental observations that the plasmon resonances of silver NPs resting on carbon films have a larger energy spread than that of silver NPs encapsulated in silicon nitride. To explain the measured optical properties of metallic NPs by using the SCRM, besides the sensitivity to particle sizes it is necessary to consider the sensitivity of optical properties to the input parameter $\hbar\omega_s$.

The primordial LSPR frequency formula Eq. (3) is extremely sensitive to energy levels of conduction electrons. However, the sufficiently precise energy levels of conduction electrons of a not-very-small metallic NP are unavailable in most cases. Fortunately, it is possible to transform Eq. (3) into an alternative form, which greatly lowers the sensitivity to the conduction electron energy levels. The calculated LSPR energies of silver NPs encapsulated in silicon nitride are not consistent with measured results except for silver NPs with radii below 2.58 nm. We think that this inconsistency occurring for not-very-small silver NPs originates from the inaccurate identification of LSPR and ASPR energies from EELS spectra. However, our calculated results perfectly explain the large energy blueshifts of few-nanometer silver NPs encapsulated in silicon nitride measured by Raza *et al.*

We also calculated the LSPR and ASPR energies of silver NPs resting on carbon films, which were studied by Scholl *et al.* We found that the ASPRs play an important role in accounting for experimental observations. Almost all measured surface plasmon resonances can be explained well by the calculated LSPRs or ASPRs, while few of the measured surface plasmons correspond to the merged resonance peaks composed of the LSPR and ASPR with similar energies of

individual silver NPs. Besides the appearance of ASPRs, the dielectric environment of silver NPs resting on carbon films changing with particle sizes is an important reason for large energy spreads of measured surface plasmon resonances. Our calculated results of silver NPs being consistent with experimental measurements further indicate that the SCRM generation mechanism and calculation scheme of ASPRs are quite reasonable and the LSPR energy shifts of metallic NPs can be calculated by using Eq. (10). We also found much larger energy blueshifts for silver NPs resting on carbon films with particle diameters in the ranges of $3.26 \text{ nm} < D < 3.32 \text{ nm}$ and $3.44 \text{ nm} < D < 3.50 \text{ nm}$, which is about twice as large as the LSPR energy blueshifts ($\sim 0.5 \text{ eV}$) observed by Scholl *et al.*

For silver NPs with radii less than 1.5 nm , our calculated LSPR energies begin to be explicitly less than the measured ones, which shows that the spherical potential well of finite depth is no longer appropriate to substitute for the effective potential V_{eff} . However, the optical properties of metallic NPs with radii less than 1.5 nm can be studied by using TD-DFT. For metallic NPs with radii larger than 20 nm , the calculations based on the SCRM are no longer time-saving. However, the optical properties of large metallic NPs can be studied by other models or theories, such as GNOR model and various QHTs. Therefore, the SCRM could serve as a bridge linking TD-DFT for very small metallic NPs with numerous models or theories for large metallic NPs.

Our calculated results have shown that within the SCRM, the optical properties of metallic NPs are completely determined by the TDSPs and NDSPs of conduction electrons, which play a central role in our calculations. To the best of our knowledge, there are no precise definitions for the NDSPs and TDSPs in the literature. We defined them by Eqs. (8) and (9), which works well going with the spherical potential well of finite depth to calculate the optical properties of metallic NPs with radii in the range $1.5 \text{ nm} < R < 20 \text{ nm}$.

APPENDIX: DERIVATION OF EQ. (10)

In this Appendix, we will derive the alternative form of Eq. (3). For two given energy levels ϵ_α and ϵ_β with $0 < \epsilon_\alpha - \epsilon_\beta \neq \hbar\Omega_p$ and the corresponding $|d_{\alpha\beta}| \neq 0$, the contribution of the energy level pair $\{\epsilon_\alpha, \epsilon_\beta\}$ to the second part $\mathcal{G}(R) = \Omega_q(R) - \Omega_p(R)$ on the right side of Eq. (3) is well over that of energy level pair $\{\epsilon_\beta, \epsilon_\alpha\}$ due to the Fermi-Dirac factor. Therefore, for each energy level pair $\{\epsilon_\alpha, \epsilon_\beta\}$ involved in the summing part of Eq. (3), we are allowed to include the contribution of energy level pair $\{\epsilon_\beta, \epsilon_\alpha\}$ to LSPR energy shifts. This procedure symmetrizes the energy-level indices of $\mathcal{G}(R)$, and the result is

$$\mathcal{G}(R) = \frac{2\mathcal{A}^2}{\hbar} \sum_{(\alpha\beta)} (f_\beta - f_\alpha) \frac{|d_{\alpha\beta}|^2 \epsilon_{\beta\alpha}}{\epsilon_{\alpha\beta}^2 - (\hbar\Omega_p)^2}. \quad (\text{A1})$$

Then, by introducing a small characteristic energy $\tau > 0$ of $\epsilon_{\alpha\beta}$ and changing $\hbar\Omega_p$ to $i\hbar\Omega$, where i is the imaginary unit ($i^2 = -1$), we can approximate the summing of $\mathcal{G}(R)$ over energy level pairs by the integral

$$\mathcal{G}(R) \approx \frac{2\mathcal{A}^2}{\hbar\tau} \int_0^Z (f_\beta - f_\alpha) \frac{|d_{\alpha\beta}|^2 \epsilon_{\alpha\beta}}{\epsilon_{\alpha\beta}^2 + (\hbar\Omega)^2} d\epsilon_{\alpha\beta}, \quad (\text{A2})$$

where Z equals to the sum of the work function and Fermi energy. We extend the integral lower limit $-Z$ and a factor $1/2$ emerges, and we change the integral variable $\epsilon_{\alpha\beta}$ to ζ . Thus, Eq. (A2) becomes

$$\mathcal{G}(R) \approx \frac{\mathcal{A}^2}{\hbar\tau} \int_{-Z}^Z (f_\beta - f_\alpha) \frac{|d_{\alpha\beta}|^2 \zeta}{\zeta^2 + (\hbar\Omega)^2} d\zeta. \quad (\text{A3})$$

We further impose on the factor $(f_\beta - f_\alpha)|d_{\alpha\beta}|^2$ suitable properties beyond the interval $(-Z, Z)$, that the integral limits can be extended to $\pm\infty$ without causing explicit variation of the integral value. Finally, we analytically continue the factor $(f_\beta - f_\alpha)|d_{\alpha\beta}|^2$ to whole complex plane. Thus, Eq. (A3) can be cast into the expression

$$\mathcal{G}(R) \approx \frac{\mathcal{A}^2}{\hbar\tau} \int_{-\infty}^{\infty} (f_\beta - f_\alpha) \frac{|d_{\alpha\beta}|^2 \zeta}{\zeta^2 + (\hbar\Omega)^2} d\zeta, \quad (\text{A4})$$

which can be calculated by using the residue theorem. There are two singular points $\pm i\hbar\Omega$ in the integrand, and the corresponding residues are the same: $(f_\beta - f_\alpha)|d_{\alpha\beta}|^2/2$. Therefore, the integrated result of Eq. (A4) is

$$\mathcal{G}(R) \approx \pm i \frac{\pi\mathcal{A}^2}{\hbar\tau} (f_\beta - f_\alpha) |d_{\alpha\beta}|^2. \quad (\text{A5})$$

The plus and minus signs, respectively, correspond to the semicircular integration contours surrounding the upper and lower complex planes.

At high temperatures, the Fermi-Dirac distribution is turned into the Boltzmann distribution. Thus, the factor $(f_\beta - f_\alpha)$ in Eq. (A5) near the singular points can be approximated by

$$f_\beta - f_\alpha \approx e^{\mu/k_B T} \frac{\zeta}{k_B T} \approx \pm i e^{\mu/k_B T} \frac{\hbar\Omega}{k_B T}. \quad (\text{A6})$$

We need to change $\hbar\Omega$ back to $\hbar\Omega_p$, namely, $\hbar\Omega \rightarrow -i\hbar\Omega_p$, thus $(f_\beta - f_\alpha)$ would obtain an extra factor $-i$ leading to Eq. (A5) becoming real, and the result is

$$\mathcal{G}(R) \approx \pm \frac{\pi\mathcal{A}^2}{\hbar\tau} (f_\beta - f_\alpha) |d_{\alpha\beta}|^2, \quad (\text{A7})$$

which shows that in this expression of LSPR energy shifts, only energy-level pairs of conduction electrons satisfying the conditions $\epsilon_{\alpha\beta} = \hbar\Omega$ and $|d_{\alpha\beta}|^2 \neq 0$ matter. Considering that there may be more than one energy-level pair satisfying these two conditions, we should sum over all such energy-level pairs and the final result is

$$\hbar\Omega_q(R) \approx \hbar\Omega_p(R) \pm \frac{\pi\mathcal{A}^2}{\tau} \sum_{(\alpha\beta)} (f_\beta - f_\alpha) |d_{\alpha\beta}|^2, \quad (\text{A8})$$

where the plus and minor signs, respectively, denote blue and red energy shifts of LSPRs.

We emphasize that the $(f_\beta - f_\alpha)$ proportional to ζ or $\epsilon_{\alpha\beta}$ in the vicinity of any one analytical point generally holds. As long as $(f_\beta - f_\alpha)$ being the complex function of ζ is analytic at a point ζ_0 , we can approximate it by the first two terms of the Taylor series near this point, that is, $(f_\beta - f_\alpha) \approx a_0 + a_1(\zeta - \zeta_0) = (a_0 - a_1\zeta_0) + a_1\zeta$, where a_0 and a_1 are

constants. It is obvious that when the variable ζ changes to $-\zeta$, $(f_\beta - f_\alpha)$ would change to $-(f_\beta - f_\alpha)$ as well, which requires $(a_0 - a_1\zeta_0)$ to be zero. Thus, $(f_\beta - f_\alpha)$ is proportional to ζ near this analytical point.

The LSPR energy shift $\mathcal{G}(R)$ could be further expressed as

$$\hbar\mathcal{G}(R) \approx \pm\pi\mathcal{A}^2(f_\beta - f_\alpha)|d_{\alpha\beta}|^2\delta(\epsilon_{\alpha\beta} - \hbar\Omega_p). \quad (\text{A9})$$

Compared with the expression of LSPR line broadening Eq. (4), the magnitude of LSPR energy shift of a not-too-small metallic NP is about half its LSPR line broadening.

The characteristic energy $\tau(\sim |\Delta\epsilon_{\alpha\beta}| \sim \Delta\epsilon_\alpha + \Delta\epsilon_\beta)$ naturally takes the minimal value of the set $\{\sqrt{4\epsilon_r\epsilon_\alpha} + \sqrt{4\epsilon_r\epsilon_\beta}\}$ of all NDSPs.

- [1] U. Kreibig and M. Vollmer, *Optical Properties of Metal Clusters* (Springer-Verlag, Berlin, 1995), and references therein.
- [2] D. K. Gramotnev, and S. I. Bozhevolnyi, Plasmonics beyond the diffraction limit, *Nat. Photonics*, **4**, 83 (2010).
- [3] P. L. Stiles, J. A. Dieringer, N. C. Shah, and R. P. Van Duyne, Surface-enhanced Raman spectroscopy, *Annu. Rev. Anal. Chem.* **1**, 601 (2008).
- [4] H. A. Atwater, and A. Polman, Plasmonics for improved photovoltaic devices, *Nat. Mater.* **9**, 205 (2010).
- [5] P. Zijlstra, P. Paulo, and M. Orrit, Optical detection of single non-absorbing molecules using the surface plasmon resonance of a gold nanorod, *Nat. Nanotech* **7**, 379 (2012).
- [6] A. V. Akimov, A. Mukherjee, C. L. Yu, D. E. Chang, A. S. Zibrov, P. R. Hemmer, H. Park, and M. D. Lukin, Generation of single optical plasmons in metallic nanowires coupled to quantum dots, *Nature (London)* **450**, 402 (2007).
- [7] D. Bar-Lev, and J. Scheuer, Plasmonic meta-surface for efficient ultra-short pulse laser-driven particle acceleration, *Phys. Rev. ST Accel. Beams*, **17**, 121302 (2014).
- [8] O. Vazquez-Mena, T. Sannomiya, L. Villanueva, J. Voros, and J. Brugger, Metallic nanodot arrays by stencil lithography for plasmonic biosensing applications, *ACS Nano*, **5**, 844 (2011).
- [9] A. Kyrsting, P. M. Bendix, D. G. Stamou, and L. B. Oddershede, Heat profiling of three-dimensionally optically trapped gold nanoparticles using vesicle cargo release, *Nano Lett.* **11**, 888 (2011).
- [10] S. Lal, S. E. Clare, and N. J. Halas, Nanoshell-enabled photothermal cancer therapy: Impending clinical impact, *Acc. Chem. Res.* **41**, 1842 (2008).
- [11] E. Kazuma, J. Jung, H. Ueba, M. Trenary, and Y. Kim, Real-space and real-time observation of a plasmon-induced chemical reaction of a single molecule, *Sci.* **360**, 521 (2018).
- [12] D. C. Marinica, M. Zapata, P. Nordlander, A. K. Kazansky, P. M. Echenique, J. Aizpurua, and A. G. Borisov, Active quantum plasmonics, *Sci. Adv.* **1**, e1501095 (2015).
- [13] G. Guzzinati, A. B  ch  , H. Lourenco-Martins, J. Martin, M. Kociak, and J. Verbeeck, Probing the symmetry of the potential of localized surface plasmon resonances with phase-shaped electron beams, *Nat. Commun.* **8**, 14999 (2017).
- [14] E. Roller, L. V. Besteiro, C. Pupp, L. K. Khorashad, A. O. Govorov, and T. Liedl, Hotspot-mediated non-dissipative and ultrafast plasmon passage, *Nat. Phys.* **13**, 761 (2017).
- [15] J. Wei, N. Jiang, J. Xu, X. Bai, and J. Liu, Strong coupling between ZnO excitons and localized surface plasmons of silver nanoparticles studied by STEM-EELS, *Nano Lett.* **15**, 5926-5931 (2015).
- [16] F. Javier Garc  a de Abajo, Optical excitations in electron microscopy, *Rev. Mod. Phys.* **82**, 209 (2010).
- [17] J. Nelayah, M. Kociak, O. St  phan, F. Javier Garc  a de Abajo, M. Tenc  , L. Henrard, D. Taverna, I. Pastoriza-Santos, L. M. Liz-Marz  n, and C. Colliex, Mapping surface plasmons on a single metallic nanoparticle, *Nat. Phys.* **3**, 348 (2007).
- [18] M. Bosman, V. J. Keast, M. Watanabe, A. I. Maarof, and M. B. Cortie, Mapping surface plasmons at the nanometre scale with an electron beam, *Nanotechnology*, **18**, 165505 (2007).
- [19] P. E. Batson, N. Dellby and O. L. Krivanek, Sub-  ngstrom resolution using aberration corrected electron optics, *Nature (London)* **418**, 617 (2002).
- [20] O. L. Krivanek, T. C. Lovejoy, N. Dellby, T. Aoki, R. W. Carpenter, P. Rez, E. Soignard, J. Zhu, P. E. Batson, M. J. Lagos, R. F. Egerton, and P. A. Crozier, Vibrational spectroscopy in the electron microscope, *Nature (London)* **514**, 209 (2014).
- [21] J. Lerm  , Size evolution of the surface plasmon resonance damping in silver nanoparticles: Confinement and dielectric effects, *J. Phys. Chem. C*, **115**, 14098 (2011).
- [22] H. Barda, P. Billaud, S. Marhaba, D. Christoulos, E. Cottancin, A. Crut, J. Lerm  , P. Maoli, M. Pellarin, M. Broyer, N. Del Fatti, F. Vall  e, A. S  nchez-Iglesias, I. Pastoriza-Santos, and M. Liz-Marz  n, Quantitative determination of the size dependence of surface plasmon resonance damping in single Ag@SiO₂ nanoparticles, *Nano Lett.* **9**, 3463 (2009).
- [23] K. L. Kelly, E. Coronado, L. L. Zhao, and G. C. Schatz, The optical properties of metal nanoparticles: The influence of size, shape, and dielectric environment, *J. Phys. Chem. B* **107**, 668 (2003).
- [24] V. Amendola, O. M. Bakr, and F. Stellacci, A study of the surface plasmon resonance of silver nanoparticles by the discrete dipole approximation method: Effect of shape, size, structure, and assembly, *Plasmonics* **5**, 85 (2010).
- [25] O. A. Yeshchenko, I. M. Dmitruk, A. A. Alexeenko, A. V. Kotko, J. Verdal, and A. O. Pinchuk, Size and temperature effects on the surface plasmon resonance in silver nanoparticles, *Plasmonics* **7**, 685 (2012).
- [26] N. W. Ashcroft and M. D. Mermin, *Solid State Physics* (Harcourt, Orlando, 1976).
- [27] J. Lerm  , B. Palpant, B. Pr  vel, M. Pellarin, M. Treilleux, J. L. Vialle, A. Perez, and M. Broyer, Quenching of the Size Effects in Free and Matrix-Embedded Silver Clusters, *Phys. Rev. Lett.* **80**, 5105 (1998).
- [28] J. Tiggesb  umker, L. K  ller, K. H. Meiwes-Broer, and A. Liebsch, Blue shift of the Mie plasma frequency in Ag clusters and particles, *Phys. Rev. A* **48**, R1749 (1993).
- [29] U. Kreibig, and L. Genzel, Optical absorption of small metallic particles, *Surf. Sci.* **156**, 678 (1985).
- [30] K. P. Charl  , L. K  nig, S. Nepijko, I. Rabin, and W. Schulze, The surface plasmon resonance of free and embedded Ag-clusters in the size range 1.5 nm < D < 30 nm, *Cryst. Res. Technol.* **33**, 1085 (1998).

- [31] R. C. monreal, T. J. Antosiewicz, S. P. Apell, Competition between surface screening and size quantization for surface plasmons in nanoparticles, *New. J. Phys.* **15**, 083044 (2013).
- [32] U. Kreibig, and C. V. Fragstein, The limitation of electron mean free path in small silver particles, *Z. Phys.* **224**, 307 (1969).
- [33] A. Kawabata, R. Kubo, Electronic properties of fine metallic particles. II. Plasma resonance absorption, *J. Phys. Soc. Jpn.* **21**, 1765 (1966).
- [34] W. A. Kraus, and G. C. Schatz, Plasmon resonance broadening in small metal particles, *J. Chem. Phys.* **79**, 6130 (1983).
- [35] S. Link, and M. A. El-Sayed, Spectral properties and relaxation dynamics of surface plasmon electronic oscillations in gold and silver nanodots and nanorods, *J. Phys. Chem. B* **103**, 8410 (1999).
- [36] G. Weick, R. A. Molina, D. Weinmann, and R. A. Jalabert, Lifetime of the first and second collective excitations in metallic nanoparticles, *Phys. Rev. B* **72**, 115410 (2005).
- [37] A. V. Uskov, I. E. Protsenko, N. A. Mortensen, and E. P. O'Reilly, Broadening of plasmonic resonance due to electron collisions with nanoparticle boundary: A quantum mechanical consideration, *Plasmonics* **9**, 185 (2014).
- [38] D. Jin, Q. Hu, D. Neuhauser, F. V. Cube, Y. Yang, R. Sachan, T. S. Luk, D. C. Bell and N. X. Fang, Quantum-Spillover-Enhanced Surface-Plasmonic Absorption at the Interface of Silver and High-Index Dielectrics, *Phys. Rev. Lett.* **115**, 193901 (2015).
- [39] N. A. Mortensen, S. Raza, M. Wubs, T. Søndergaard, and S. I. Bozhevolnyi, A generalized non-local optical response theory for plasmonic nanostructures, *Nat. Commun.* **5**, 3809 (2014).
- [40] S. Raza, S. I. Bozhevolnyi, M. Wubs, and N. A. Mortensen, Nonlocal optical response in metallic nanostructures, *J. Phys: Cond. Matter.* **27**, 183204 (2015).
- [41] A. Liebsch, Surface-plasmon dispersion and size dependence of Mie resonance: Silver versus simple metals, *Phys. Rev. B* **48**, 11317 (1993).
- [42] P. Apell, and A. Ljungbert, Red shift of surface plasmons in small metal particles, *Solid State Commun.* **44**, 1367 (1982).
- [43] T. Christensen, W. Yan, S. Raza, A. P. Jauho, N. A. Mortensen, and M. Wubs, Nonlocal response of metallic nanospheres probed by light, electrons and atoms, *ACS Nano.* **8**, 1745 (2014).
- [44] R. Ruppín, Optical Properties of a Plasma Sphere, *Phys. Rev. Lett.* **31**, 1434 (1973).
- [45] K. Kolwas, and A. Derkachova, Plasmonic abilities of gold and silver spherical nanoantennas in terms of size dependent multipolar resonance frequencies and plasmon damping rates, *Opto-Electr. Rev.* **18**, 429 (2010).
- [46] S. Raza, S. Kadkhodazadeh, T. Christensen, M. D. Vece, M. Wubs, N. A. Mortensen, and N. Stenger, Multipole plasmons and their disappearance in few-nanometer silver nanoparticles, *Nat. Commun.* **6**, 8788 (2015).
- [47] J. A. Scholl, A. L. Koh, and J. A. Dionne, Quantum plasmon resonances of individual metallic nanoparticles, *Nature (London)* **483**, 421 (2012).
- [48] S. Raza, N. Stenger, S. Kadkhodazadeh, S. V. Fischer, N. Kosterha, A. P. Jauho, A. Burrows, M. Wubs, and N. A. Mortensen, Blueshift of the surface plasmon resonance in silver nanoparticles studied with EELS, *Nanophotonics* **2**, 131 (2013).
- [49] E. Runge, and E. K. U. Gross, Density-Functional Theory for Time-Dependent Systems, *Phys. Rev. Lett.* **52**, 997 (1984).
- [50] G. Vignale, C. A. Ullrich, and S. Conti, Time-Dependent Density Functional Theory Beyond the Adiabatic Local Density Approximation, *Phys. Rev. Lett.* **79**, 4878 (1997).
- [51] G. Toscano, J. Straubel, A. Kwiatkowski, C. Rockstuhl, F. Evers, H. Xu, N. A. Mortensen, and M. Wubs, Resonance shifts and spill-out effects in self-consistent hydrodynamic nanoplasmonics, *Nat. Commun.* **6**, 7132 (2015).
- [52] C. Ciraci, Current-dependent potential for nonlocal absorption in quantum hydrodynamic theory, *Phys. Rev. B* **95**, 245434 (2017).
- [53] C. Ciraci, and F. D. Sala, Quantum hydrodynamic theory for plasmonics: The impact of the electron density tail, *Phys. Rev. B* **93**, 205405 (2016).
- [54] W. Yan, Hydrodynamic theory for quantum plasmonics: Linear-response dynamics of the inhomogeneous electron gas, *Phys. Rev. B* **91**, 115416 (2015).
- [55] T. V. Teperik, P. Nordlander, J. Aizpurua, and A. G. Borisov, Robust Subnanometric Plasmon Ruler by Rescaling of the Nonlocal Optical Response, *Phys. Rev. Lett.* **110**, 263901 (2013).
- [56] G. Weick, C. Woollacott, W. L. Barnes, O. Hess, and E. Mariani, Dirac-Like Plasmons in Honeycomb Lattices of Metallic Nanoparticles, *Phys. Rev. Lett.* **110**, 106801 (2013).
- [57] M. Brack, The physics of simple metal clusters: Self-consistent jellium model and semiclassical approaches, *Rev. Mod. Phys.* **65**, 677 (1993).
- [58] W. Ekaradt, Size-dependent photoabsorption and photoemission of small metal particles, *Phys. Rev. B* **31**, 6360 (1985).
- [59] C. Yannouleas, E. Vigezzi, and R. A. Broglia, Evolution of the optical properties of alkali-metal microclusters towards the bulk: The matrix random-phase approximation description, *Phys. Rev. B* **47**, 9849 (1993).
- [60] V. H. Nguyen, and B. H. Nguyen, Basics of quantum plasmonics, *Adv. Nat. Sci: Nanosci. Nanotechnol.* **6**, 023001 (2015).
- [61] G. Wang, Y. Zheng, and J. Zi, Discontinuous variation of the surface plasmon linewidth of small sodium nanoparticles with electron temperatures, *Europhys. Lett.* **110**, 37009 (2015).
- [62] G. Weick, Quantum dissipation and decoherence of collective excitations in metallic nanoparticles, Ph.D. thesis defence in Strasbourg, 22 September 2006 in front of the jury comprising, Université Louis Pasteur (unpublished).
- [63] G. Weick, G. L. Ingold, R. A. Jalabert, and D. Weinmann, Surface plasmon in metallic nanoparticles: Renormalization effects due to electron-hole excitations, *Phys. Rev. B* **74**, 165421 (2006).
- [64] M. Barbry, P. Koval, F. Marchesin, R. Esteban, A. G. Borisov, J. Aizpurua, and D. Sánchez-Portal, Atomistic near-field nanoplasmonics: Reaching atomic-scale resolution in nano-optics, *Nano Lett.* **15**, 3410 (2015).
- [65] The radial wave function of a conduction electron outside the nanosphere is $\propto \frac{1}{\sqrt{V}} f_{\alpha}(k_{\alpha} r) e^{-k_{\alpha} r}$, where $V = \frac{4}{3}\pi R^3$ is the volume of the metallic nanosphere, and k_{α} the wave vector. The matrix element can be calculated in the effective region $r > R + \delta$, where $\delta \ll R$ is the uncertainty of the particle radius,

as

$$d_{\alpha\beta} \propto \frac{1}{V} \int_{R+\delta}^{\infty} f_{\alpha}(k_{\alpha}r) \left(\frac{R^3}{r^3} - 1\right) f_{\beta}(k_{\beta}r) r^3 dr.$$

Letting $t = r/R$ and $x = t - (1 + \delta/R)$, the matrix element can be expressed as $d_{\alpha\beta} \approx \kappa R + \lambda$. Considering the coefficient $\mathcal{A}^2 \propto 1/R^3$ and $N_{out} \propto \varrho R + \sigma R^2$ given by the similar calculation, we obtain the size dependence of the LSPR energy $\hbar\Omega_q(R) = \hbar\omega_M + \frac{E}{R} + \frac{K}{R^2} + \frac{S}{R^3}$. The LSPR line broadening proportional to $\mathcal{A}^2 |d_{\alpha\beta}|^2$ also obeys the same relationship.

- [66] S. Peng, J. M. McMahon, G. C. Schatz, S. K. Gray, and Y. Sun, Reversing the size-dependence of surface plasmon resonances, *Proc. Natl. Acad. Sci. USA* **107**, 14530 (2010).
- [67] A. J. Bennett, Influence of the electron charge distribution on surface-plasmon dispersion, *Phys. Rev. B* **1**, 203 (1970).
- [68] K. D. Tsuei, E. W. Plummer, A. Liebsch, K. Kempa, and P. Bakshi, Multipole Plasmon Modes at a Metal Surface, *Phys. Rev. Lett.* **64**, 44 (1990).

- [69] G. Wang, H. Li, Y. Shen, and B. Dong, New approximate method to solve the Schrödinger equation with a Woods-Saxon-like potential, *J. Math. Phys.* **52**, 112105 (2011).
- [70] H. Nishioka, K. Hansen, and B. R. Mottelson, Supershells in metal clusters, *Phys. Rev. B* **42**, 9377 (1990).
- [71] T. L. Ferrell, R. J. Warmack, V. E. Anderson, and P. M. Echenique, Analytical calculation of stopping power for isolated small spheres, *Phys. Rev. B* **35**, 7365 (1987).
- [72] A. D. Rakić, A. B. Djurišić, J. M. Elazar, and M. L. Majewski, Optical properties of metallic films for vertical-cavity optoelectronic devices, *Appl. Opt.* **37**, 5271 (1998).
- [73] To calculate the LSPR energies by using Eq. (10), we first calculate the contribution of each NDSP to the LSPR energy shift by using Eq. (3); second, if any two NDSPs not being TDSPs have opposite contributions $E_{\xi\zeta}$ and $E_{\mu\nu}$ satisfying the condition $|E_{\xi\zeta} + E_{\mu\nu}| / \max[E_{\xi\zeta}, E_{\mu\nu}] < 0.2$, then two such NDSPs do not contribute to the LSPR energy shift. Finally, the rest of the NDSPs produce the LSPR energy shift according to Eq. (10).